Journal of Power Sources 263 (2014) 66–74

Contents lists available at ScienceDirect

Journal of Power Sources

journal homepage: www.elsevier.com/locate/jpowsour

Fluorinated phosphazene co-solvents for improved thermal and safety performance in lithium-ion battery electrolytes

Harry W. Rollins*, Mason K. Harrup, Eric J. Dufek, David K. Jamison, Sergiy V. Sazhin, Kevin L. Gering, Dayna L. Daubaras

Idaho National Laboratory, P.O. Box 1625, Idaho Falls, ID 83415, USA

HIGHLIGHTS

- Fluorinated cyclic phosphazene electrolytes for lithium-ion batteries.
- Improved thermal and safety performance.
- Improved electrochemical window.
- Comparable rate capabilities at C/1 for up to 20 wt% phosphazene.

ARTICLE INFO

Article history:
Received 5 March 2014
Received in revised form
3 April 2014
Accepted 4 April 2014
Available online 16 April 2014

Keywords:
Phosphazene
Electrolyte
Lithium-ion battery
Stability
Non-flammable

ABSTRACT

The safety of lithium-ion batteries is coming under increased scrutiny as they are being adopted for large format applications especially in the vehicle transportation industry and for grid-scale energy storage. The primary short-comings of lithium-ion batteries are the flammability of the liquid electrolyte and sensitivity to high voltage and elevated temperatures. We have synthesized a series of non-flammable fluorinated phosphazene liquids and blended them with conventional carbonate solvents. While the use of these phosphazenes as standalone electrolytes is highly desirable, they simply do not satisfy all of the many requirements that must be met such as high $LiPF_6$ solubility and low viscosity, thus we have used them as additives and co-solvents in blends with typical carbonates. The physical and electrochemical properties of the electrolyte blends were characterized, and then the blends were used to build 2032-type coin cells. We have evaluated the performance of the electrolytes by determining the physical properties, thermal stability, electrochemical window, cell cycling data, and the ability to form solid electrolyte interphase (SEI) films. This paper presents our most recent results on a new series of fluorinated cyclic phosphazene trimers, the FM series, which has exhibited numerous beneficial effects on battery performance, lifetimes, and safety aspects.

1. Introduction

As lithium-ion batteries are being rapidly adopted for large format applications, the safety of these systems is receiving ever-increasing scrutiny. More stringent safety and energy density requirements make the development of electrolytes with lower flammability, larger electrochemical window, and higher operating voltages a necessity [1]. Most of the commercial electrolytes for lithium-ion batteries are $LiPF_6$ dissolved in a mixture of organic carbonate and/or ester solvents [2]. These electrolyte blends are highly volatile and highly flammable, with typical flash points of around 30 °C or less. This presents serious safety concerns especially when utilized in large format cells or when the cells come under undo stress or physical damage. One approach to improve the safety performance of the electrolyte is to use additives and co-solvents to reduce the flammability of the organic carbonate and ester electrolytes. A variety of additives and co-solvents have been proposed, including sulfones, ionic liquids, phosphates, phospholanes, phosphazenes, siloxanes, fluorinated carbonates, and fluorinated ethers and mixtures thereof [3–10]. In addition to flammability suppression, additives have also been used to improve solid electrolyte interphase (SEI) formation [11], overcharge protection [12], and thermal stability [13]. Compared to other organophosphorous compounds and other additives, phosphazenes showed the least degradation in battery performance [14]. We have

* Corresponding author. Tel.: +1 208 526 4066.
E-mail address: harry.rollins@inl.gov (H.W. Rollins).

http://dx.doi.org/10.1016/j.jpowsour.2014.04.015
0378-7753/

Table 1
Pendant group distribution and properties of the FM series of phosphazenes.

Designation	# of 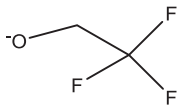	# of 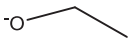	Average molecular weight (g mol^{-1})	Density (g ml^{-1})
FM1	6	0	729.13	n.d[a]
FM2	3	3	567.22	1.33
FM3	2	4	513.25	1.28
FM4	1	5	459.27	1.29

[a] Not determined.

focused our recent investigations on the use of novel low molecular weight phosphazenes as additives and co-solvents in lithium ion batteries [15–18]. This paper presents our results on a series of chemically similar, fluorinated cyclic phosphazene trimers, referred to as the FM series in this paper.

2. Experimental

2.1. Instrumentation

During the synthesis of the phosphazenes the reaction progress was followed by ^{31}P NMR using a Bruker Avance III 600 MHz spectrometer. To ensure the materials were dry, titrations were performed using a Mettler Toledo C30 Karl Fischer coulometer (in an argon glovebox). To ensure the samples were halide-free, samples were analyzed by ion-chromatography with a conductivity detector. Electrolyte blends containing the fluorinated phosphazenes, alkyl carbonates and $LiPF_6$ were prepared in an argon glovebox where the conductivity and viscosity were determined. The reported conductivities are the average of ten measurements obtained on a TOA CM-30R conductivity meter. The viscosities of the blends were determined using a Cambridge DL-4100 (falling bob) viscometer (average of 10 measurements). A portion of the sample was passed out of the glovebox, where the flash point and vapor pressure were determined. Closed-cup flash points were determined using a Setaflash 82000-0 (electric ignition) using a ramp determination method. Vapor pressures of the samples were determined from 15 °C to 60 °C in 1 °C increments using a Grabner Instruments Minivap VPXpert vapor pressure analyzer. Thermal stability experiments were run in an ESPEC BTU133 thermal chamber.

2.2. Reagents

Hexachlorocyclotriphosphazene was obtained from Molport.com and was purified by sublimation prior to use. Anhydrous ethanol, anhydrous 1,4-dioxane, dichloromethane, and sodium metal were obtained from Sigma–Aldrich and were used as received. 2,2,2-trifluoroethanol (Sigma–Aldrich) was distilled prior to use. Battery-grade $LiPF_6$, ethylene carbonate (EC), ethyl methyl carbonate (EMC), and diethyl carbonate (DEC) were obtained from Kishida Chemical Co. and were used as received in an argon glovebox.

2.3. Synthesis of the fluorinated phosphazenes

We prepared a series of chemically similar fluorinated cyclic phosphazene trimers with varying number of fluorinated pendant groups. This series of compounds was prepared by the nucleophilic substitution of the reactive chlorines on hexachlorocyclotriphosphazene with ethoxy or 2,2,2-trifluoroethoxy groups. The number of ethoxy and 2,2,2-trifluoroethoxy groups where varied as shown in Table 1. Fig. 1 shows the structure for FM2 as an example. Synthesis of this series of fluorinated phosphazenes were carried out in oven dried glassware under a blanket of nitrogen gas using Schlenk techniques. The synthesis of each of these materials were nearly identical, the details of the FM2 synthesis are given below.

2.3.1. Sodium ethoxide

An oven-dried 1 L 3-neck flask was fitted with a dry nitrogen inlet, a reflux condenser and rubber septa. The dry nitrogen outlet was fitted to the top of the reflux condenser and passed through a bubbler filled with ~2 inches of silicon oil. The reactor was kept under a slow steady stream of dry nitrogen until the completion of the reaction. The flask was filled with ~700 ml of anhydrous dioxane and then 9.92 g sodium metal (0.431 mol) was added. To this a 60% excess of ethanol was added (40 ml, 0.685 mol). The reaction was heated at sub-reflux temperature until all of the sodium was consumed.

2.3.2. Sodium trifluoroethoxide

An oven-dried, 2 L 3-neck flask was fitted with a dry nitrogen inlet, a reflux condenser and rubber septa. The dry nitrogen outlet was fitted to the top of the reflux condenser and passed through a bubbler filled with ~2 inches of silicon oil. The reactor was kept under a slow steady stream of dry nitrogen till the completion of the reaction. The flask was filled with ~700 ml of anhydrous dioxane and then 11.3 g sodium metal (0.49 mol) was added. Then 35.7 ml (0.49 mol) of the TFE was added. The reaction was heated at nearly reflux temperature until all of the sodium was consumed.

2.3.3. Hexachlorocyclotriphosphazene substitution

In an oven dried 500 ml flask, 50 g (0.144 mol) of the hexachlorocyclotriphosphazene trimer was dissolved in ~300 ml anhydrous dioxane which was then added to the sodium ethoxide solution (under nitrogen at room temperature) and heated at sub-reflux for 5 h and the reaction progress was monitored by ^{31}P NMR. This solution was then cooled to room temperature and then added to the sodium trifluoroethoxide (at RT under nitrogen). This solution was heated to sub reflux for ~5 h. This reaction was also followed by ^{31}P NMR. When the reaction was complete, the solution was allowed to cool to room temperature and the excess ethoxides were quenched with water. The solution was neutralized with 2 M HCl. The solvent was removed by rotary evaporation leaving the FM product (a liquid) and undissolved solid sodium chloride. The

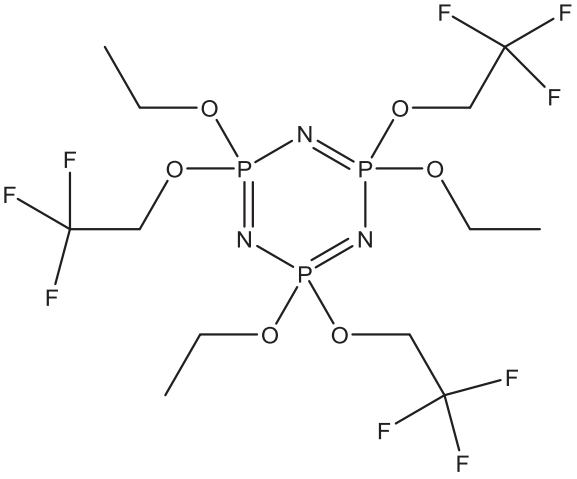

Fig. 1. Structure of the fluorinated phosphazene designated FM2.

product separated from the salt by decantation and taken up in dichloromethane and washed with nanopure (18 MΩ cm) water in a separatory funnel six times to remove trace impurities. The dichloromethane was removed from the product on a rotary evaporator and the product was then dried in an argon purged vacuum oven for several days, refreshing the atmosphere with fresh UHP argon daily. The sample was then analyzed for Cl^- by ion-chromatography and for water by Karl Fisher titration.

2.4. Coin cell construction and testing

Each of the electrolyte chemistries of interest was evaluated in full cells using CR 2032 coin cell hardware. Cells were constructed using a G8 (Conoco-Phillips) graphite based anode and a blended $Li_{1.06}Mn_{1.94}O_4$ + $Li_{1.1}Ni_{0.33}Mn_{0.33}Co_{0.33}O_2$ cathode. The geometric area of each electrode was 1.43 cm^2. A Celgard 2325 separator (1.58 cm^2) was used to separate the electrodes.

Prior to building cells, all non-separator components were dried overnight at 90 °C under vacuum. Separators were dried at 60 °C under vacuum overnight. All cells were built in an Ar atmosphere with oxygen and water content at or below 0.1 ppm. During the build process both the anode and cathode were flooded with electrolyte to ensure uniform electrolyte distribution within each electrode. To ensure reproducibility, all cell formulations were evaluated in triplicate. Following construction, stainless steel tabs were spot welded onto the positive and negative terminals of the cell respectively prior to mounting in a cell holder which was designed and built in house.

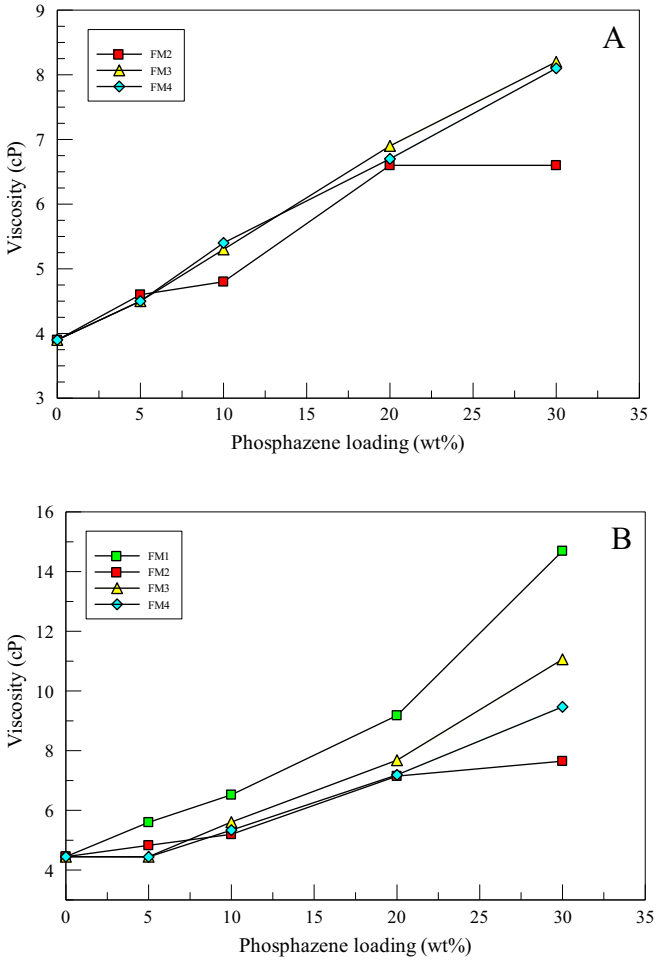

Fig. 2. Viscosity as a function of phosphazene loading in A) 1:1 EC:DEC with 1.0 M $LiPF_6$ and in B) 1:2 EC:EMC with 1.2 M $LiPF_6$.

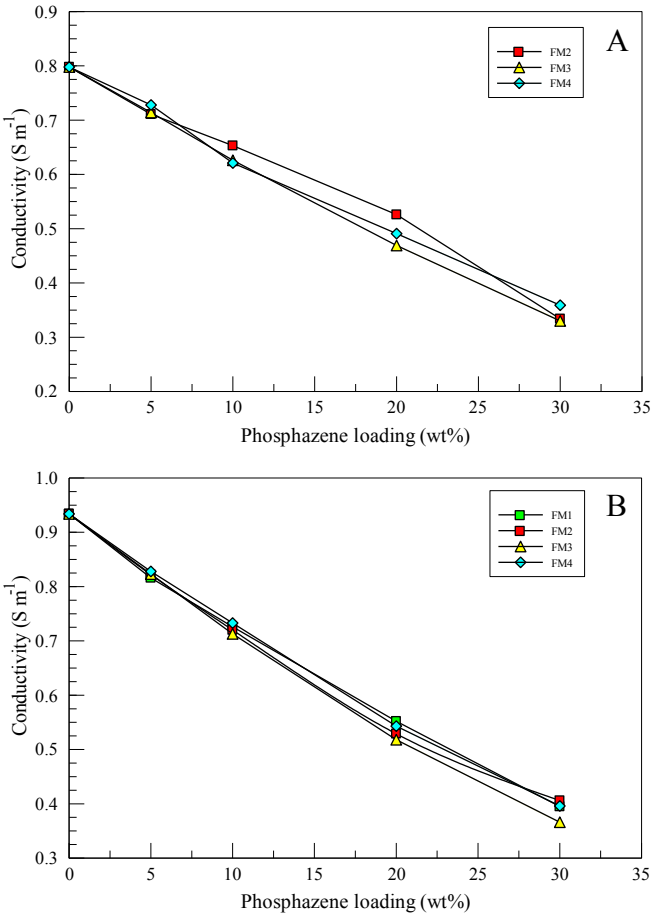

Fig. 3. Conductivity as a function of phosphazene loading in A) 1:1 EC:DEC with 1.0 M $LiPF_6$ and in B) 1:2 EC:EMC with 1.2 M $LiPF_6$.

The holder maintained the cells in a horizontal position with only slight tilting in any one direction. Within the holder, each cell was spaced a minimum of 5 cm from its nearest neighbor with open space on all sides. This orientation is preferred to minimize potential pooling of electrolyte within the cell and to provide a uniform thermal profile from cell to cell. The holders with the cells were placed in the environmental chambers (Tenney or Espec) and allowed to equilibrate to 30 °C over 2 h before testing. Cells were maintained at this temperature (30 °C) during the entire testing time. Full cell testing was performed using a 4000 Series Maccor test system that included up-front formation cycling based on C/10 constant-current (CC) conditions, and other CC conditions to determine aging behavior and sensitivity of cell performance to rate. Typical cycling occurred between 3.0 and 4.2 V at various cycling rates. Prior to initiating the testing protocol, each Maccor channel was calibrated. Electrochemical impedance spectroscopy (EIS) data was acquired using a Solartron SI 1287 Electrochemical Interface and a Solartron SI 1260 Impedance/Gain-phase analyzer. EIS data were acquired at open circuit after discharging the cell to 3.75 V and then charging to 3.9 V and were taken at frequencies ranging from 0.1 to 100,000 Hz with 20 mV amplitude.

3. Results and discussion

3.1. Physical property measurements of the phosphazenes

Once the fluorinated phosphazene additives were found to be chloride free and dry, they were immediately blanketed in argon

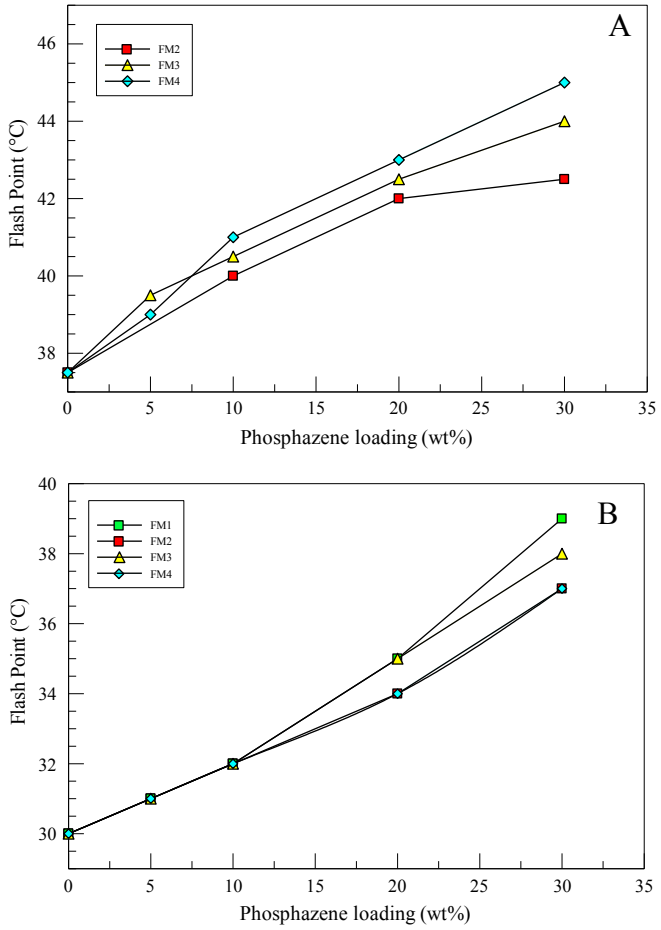

Fig. 4. Flash point as a function of phosphazene loading in A) 1:1 EC:DEC with 1.0 M $LiPF_6$ and in B) 1:2 EC:EMC with 1.2 M $LiPF_6$ compared to the baseline electrolytes.

and transferred to an argon glovebox. Two different carbonate based blends were chosen for comparison, the first was 1:1 (wt/wt) EC:DEC with 1.0 M $LiPF_6$ (baseline A), and the second baseline blend (baseline B) was 1:2 (v/v) EC:EMC with 1.2 M $LiPF_6$. Blends of these baseline electrolytes containing various concentrations of up to 30 wt% of the fluorinated phosphazenes were prepared individually, taking care to keep the overall $LiPF_6$ concentration constant (at either 1.0 M or 1.2 M). Fig. 2 shows the viscosities of the electrolyte blends containing 0, 5, 10, 20, and 30 wt% of each of the fluorinated phosphazenes. The viscosities of the neat phosphazene liquids were too high (~50 cP) to be used as standalone electrolytes. The viscosity of each of the blends systematically increased with increasing phosphazene loading. The viscosities of both of the baseline electrolytes are approximately 4 cP and increased up to approximately 10 cP for the samples containing 30% phosphazene. The exception to this was FM1, which has a melting point near room temperature. The viscosities of the blends with FM1 were systematically higher than the blends with FM2, FM3, and FM4.

Fig. 3 presents the results of conductivity measurements of the blends for the various fluorinated phosphazenes. The conductivity of baseline B is 0.934 S m^{-1} compared to 0.798 S m^{-1} for baseline A as would be expected due to the difference in $LiPF_6$ concentrations (1.0 M vs. 1.2 M). In both of the baseline electrolytes the overall conductivity decreases with increase in the phosphazene loading and is primarily due to the direct influence of increased viscosity. Even with phosphazene loadings of 30%, the conductivities of the electrolytes are above 0.3 S m^{-1}. The degree of fluorination appears to have little effect on the conductivity as can be seen by comparing the results for FM1, FM2, FM3, and FM4.

After conductivity and viscosity measurements were determined, samples of the electrolyte blends were passed out of the glovebox and the flash point and vapor pressures were immediately determined. The flash points of the blends are shown in Fig. 4. The baseline A blend had a flash point of 37.5 °C. In blend A the flash point was systematically increased with increased loading of the phosphazene, up to 44.5 °C for the blend with 30% FM4. The effectiveness of the phosphazenes was FM4, followed by FM3, and then FM2. This corresponds to decreasing number of trifluoroethoxy groups on the phosphazene and increasing number of ethoxy groups. This suggests that the phosphazenes are interacting with and suppressing the flammability of the more flammable DEC (DEC fp = 25 °C, EC fp = 143 °C; [19]) component of the blend. The flash point of blend B baseline electrolyte was 30 °C, which is 1:2 EC:EMC. The flash point for the more flammable component in blend B, the EMC, is 23.9 °C [19]. Baseline B is more flammable than baseline A due to the larger proportion of the more volatile component. The addition of phosphazenes to this baseline electrolyte also showed higher flash points with increasing proportion of phosphazene. For the blends with 30% phosphazene the flash point increased from 30 °C to 37.0 °C for FM2 and FM4, 38.0 °C for FM3, and 39.0 °C for FM1.

The vapor pressures, as a function of temperature, of the electrolyte blends with each of the phosphazenes (at 20%) are shown in

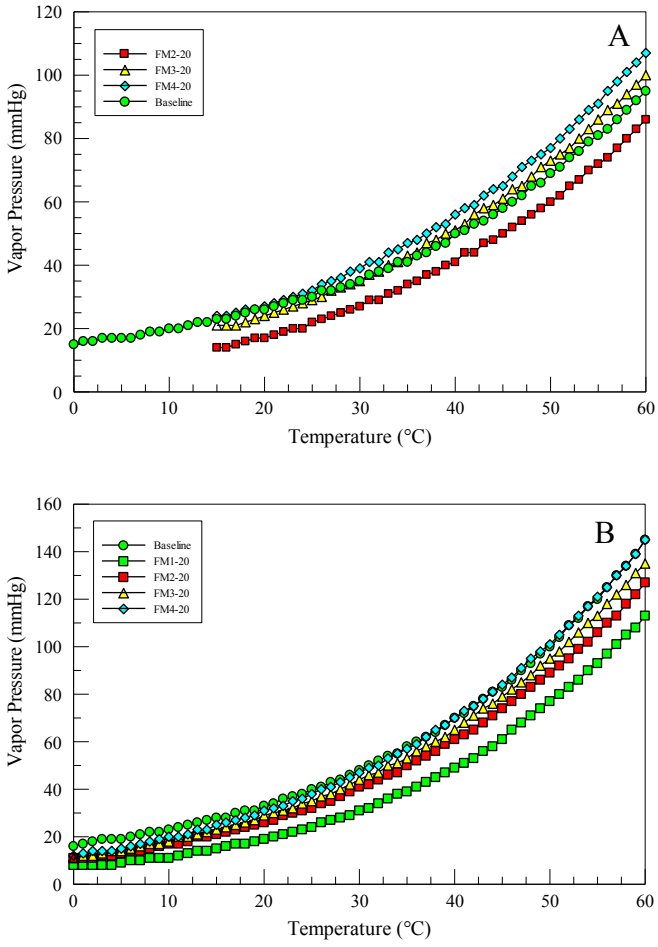

Fig. 5. Vapor pressures of electrolyte blends containing 20 wt% of each of the phosphazenes in A) 1:1 EC:DEC with 1.0 M $LiPF_6$ and in B) 1:2 EC:EMC with 1.2 M $LiPF_6$ compared to the baseline electrolytes.

Table 2
Composition of electrolyte blends containing 20 wt% phosphazene and vapor pressures at 30 °C.

	Mole fraction			Vapor pressure (mmHg)
	Phosphazene	DEC/EMC	$^{-}OCH_2CF_3$	
Baseline A	0	0.355	0	35
FM2	0.048	0.338	0.144	27
FM3	0.051	0.337	0.102	35
FM4	0.057	0.335	0.057	39
Baseline B	0	0.563	0	48
FM1	0.032	0.545	0.193	24
FM2	0.049	0.536	0.146	32
FM3	0.052	0.534	0.103	35
FM4	0.058	0.530	0.058	38

Fig. 5. In baseline A, at phosphazene concentrations of 20% and 30%, the electrolyte formed two separate liquid phases at low temperature. For electrolyte blends in baseline A, vapor pressure measurements were started at 15 °C, for all other samples vapor pressures were determine from 0 °C to 60 °C. In baseline A, FM2 depressed the vapor pressure somewhat. The vapor pressure for 20% FM3 is nearly identical to the baseline, while for 20% FM4 the vapor pressure is actually slightly higher which could be explained if there is preferential solvation between FM4 and the less volatile EC. The vapor pressures for baseline B are higher than the corresponding samples in baseline A due to the larger proportion of the more volatile component, EMC. All of the phosphazenes were effective at lowering the vapor pressure compared to the baseline electrolyte. The vapor pressure of the electrolyte blends followed the order: baseline ≥ FM4 > FM3 > FM2 > FM1. As the number of trifluoroethoxy groups on the phosphazene core (and hence the molecular weight of the phosphazene) increased, the vapor pressure of the electrolyte blend decreased.

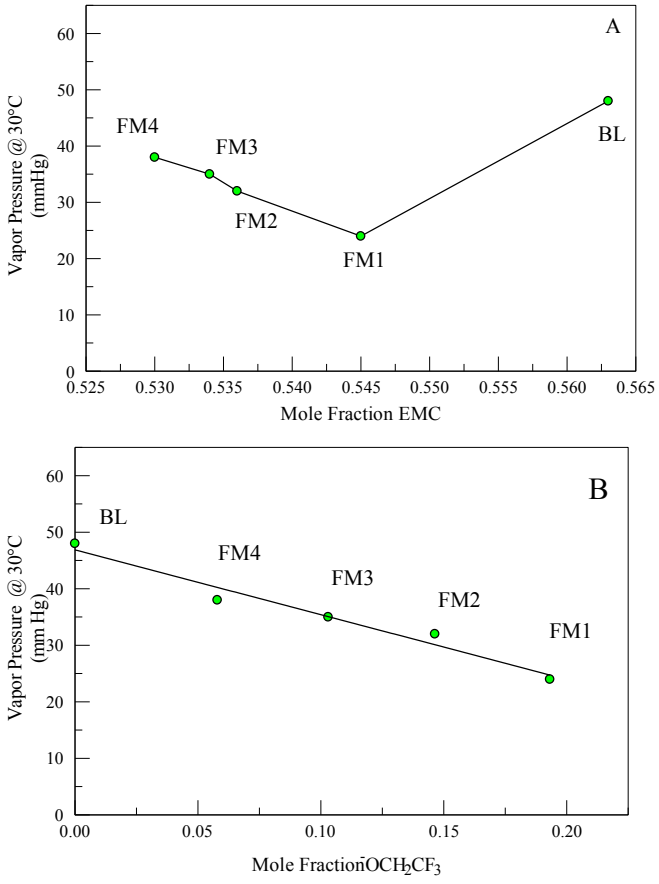

Fig. 6. Vapor pressures for 20 wt% phosphazenes in baseline B at 30 °C as a function of A) mole fraction EMC and B) mole fraction of $^{-}OCH_2CF_3$.

Because the phosphazenes and the ethylene carbonate are relatively non-volatile, the vapor pressures of the blends should be proportional to the mole fraction of the volatile component (DEC or EMC for baselines A and B respectively). Because the blends were prepared on a weight percentage basis, the number of moles of the phosphazene added varied due to the differences in molecular weight. Table 1 gives the molecular weights and densities for each of the phosphazenes. The mole fraction of each of the components of the blends and the vapor pressure at 30 °C for the 20% phosphazene blends is shown in Table 2. The mole fraction of the phosphazene varied from 0.032 to 0.058, however the variation of the volatile components (DEC and EMC) varied only slightly. While the data in baseline A are somewhat scattered, the data for baseline B is quite clear (Fig. 6). Fig. 6 shows the vapor pressures of the blends (at 30 °C) plotted versus the mole fraction of EMC and mole fraction of the trifluoroethoxy groups. While the baseline has the highest mole fraction of EMC (0.563) and the highest vapor pressure (48 mmHg), the vapor pressures of the blends containing phosphazene actually decrease with increasing EMC mole fraction. Fig. 6B shows that the vapor pressures of the blends decrease linearly with increasing mole fraction of trifluoroethoxy groups.

3.2. Thermal behavior of electrolytes with the phosphazenes

Cyclic phosphazene trimers have negligible volatility and extremely high thermal stability, not undergoing decomposition until approximately 270 °C. Our previous work with other cyclic phosphazene trimers showed that not only were they thermally stable, but that they actually enhanced the thermal stability of the blends with conventional carbonate electrolytes [17]. In order to determine if the FM series of phosphazenes could also enhance the thermal stability of the blends a sample of each of the electrolyte blends (in a hermetically sealed vial) was placed in an environmental chamber at 60 °C and was periodically inspected and photographed. Fig. 7 shows a series of photographs over time of 10% of each of the phosphazenes FM2, FM3, and FM4 in both of the baseline electrolytes as well as the baselines without any phosphazene. Both of the baseline electrolytes showed visible discoloration within the first 2 weeks. Blends containing phosphazenes initially showed no discoloration (FM2 and FM3) or very little for the case of FM4. By day 42, both of the baseline electrolytes are a deep red and by day 55, they are black, very viscous, with the formation of copious amounts of solid precipitate. The decreased volume of the baseline electrolytes in the later images is not due to evaporation of solvent, but is due to the formation of the solid precipitates, the volume of the samples containing the phosphazenes remains constant throughout the testing. Oxygen is also not expected to have an effect as the integrity of the crimp-sealed vials remained intact as evidenced by the lack of evaporation. By day 55, the samples containing phosphazenes show very little if any change, while the baseline blends are solid residues. By day 98, even the blends with the phosphazenes are showing a slight discoloration which becomes more pronounced by day 245. All of the phosphazenes greatly increased the thermolytic stabilities of the blends for both of the baseline electrolytes, with FM2 being the most effective. Our previous work has shown that as little as 1% phosphazene is enough to provide this thermal stability [17]. Ongoing multidimensional NMR experiments indicate the stabilization is provided by the phosphazene due to their ability to act as a free-radical sponge, thus preventing the polymerization of the EC and other carbonate electrolytes.

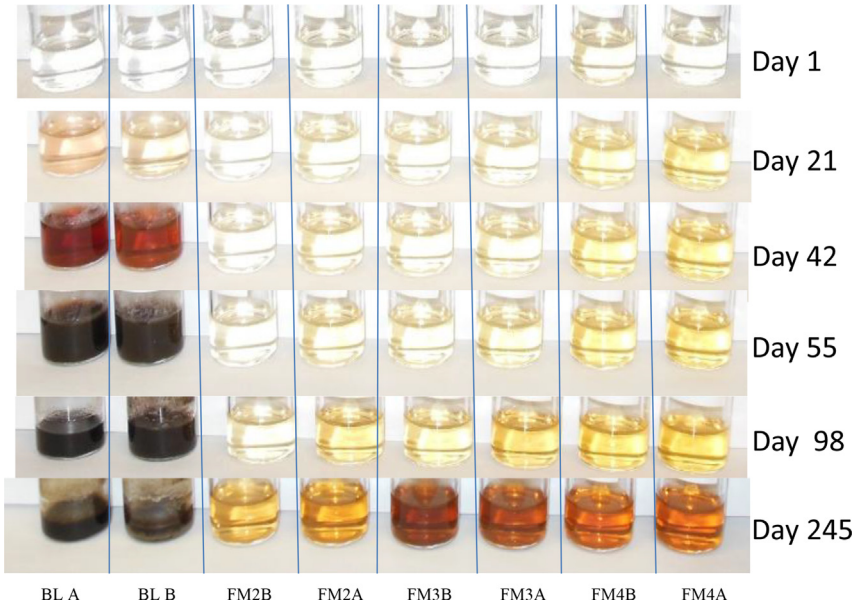

Fig. 7. Thermolytic stability of 10 wt% phosphazene blends in baseline A (BL A) 1:1 EC:DEC with 1.0 M $LiPF_6$ and in baseline B (BL B) 1:2 EC:EMC with 1.2 M $LiPF_6$ compared to the baseline electrolyte.

3.3. *Electrochemical characterization*

The electrochemical stability of the FM series of phosphazenes (20 wt%) with 80 wt% 1:4 EC:EMC with 1.2 M $LiPF_6$ was examined. One of the metrics of stability is the electrochemical window (EW). The EW is the potential region were no redox reactions occur in the electrolyte itself. There are a number of methods reported in the literature for determining the electrochemical window, however all of them are relative and vary based on the assumptions made. Our method is sensitive enough to observe differences in the electrochemical window for each of the phosphazene blends. To measure the EW, two separate potentiodynamic polarizations were done. One polarization used nickel metal foil as the working electrode against lithium counter and lithium reference electrodes at potentials negative to OCV. Another polarization used aluminum metal foil as the working electrode against lithium counter and lithium reference electrodes at potentials positive to OCV. A combination of potentiodynamic polarization curves, on Ni and Al, on the same potential scale against Li, allows the EW to be estimated

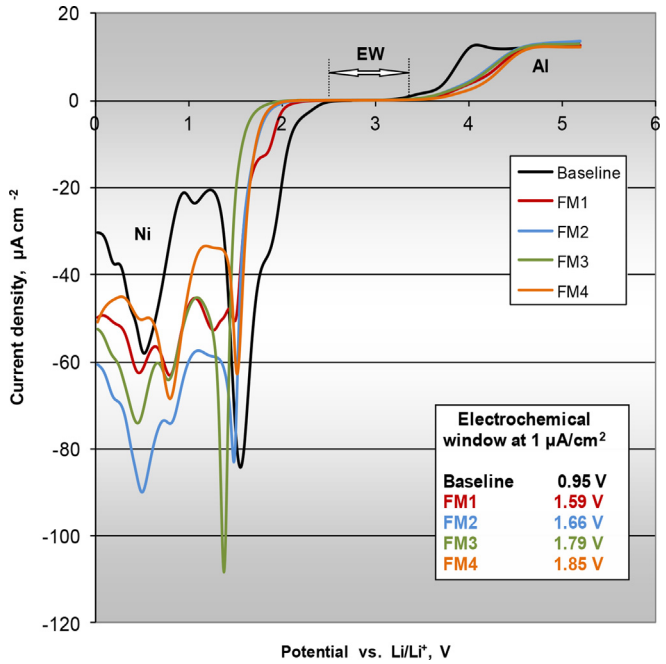

Fig. 8. Voltammogram of 20 wt% phosphazene, 80 wt% 1:4 EC:EMC blends with overall 1.2 M $LiPF_6$.

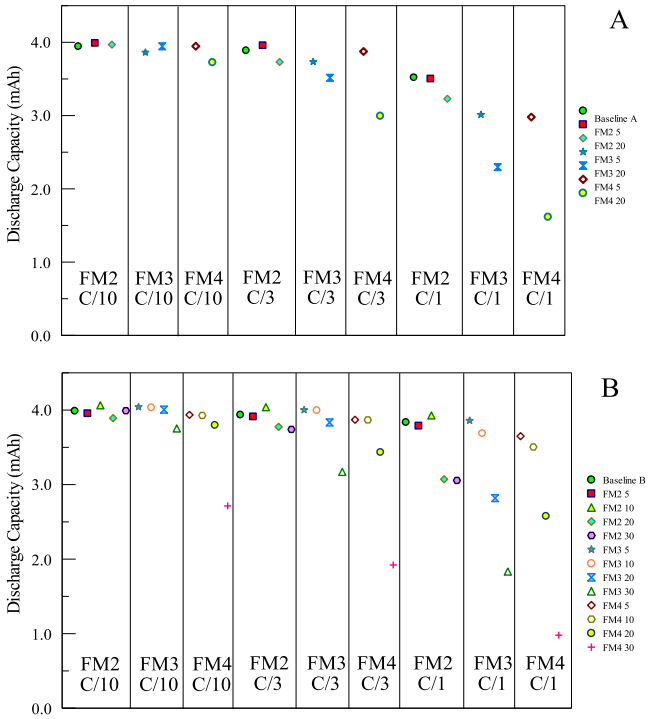

Fig. 9. Average initial discharge capacities for cells at different rates in A) 1:1 EC:DEC with 1.0 M $LiPF_6$ and in B) 1:2 EC:EMC with 1.2 M $LiPF_6$ compared to the baseline electrolytes.

for the electrolyte solutions, Fig. 8. A 1 μA current limit was used as a metric for EW evaluation. The EW for the baseline alone is 0.95 V. Addition of each of the phosphazenes dramatically increases the EW to as high as 1.85 V, adding nearly 1 V of stability to the electrolyte blend. All of the FMs were effective in expanding the EW; however those with a lower degree of fluorination were more effective.

An assessment of phosphazene-based electrolytes in regards to film formation capability (SEI on anode and cathode-electrolyte interface on cathode) was performed, the results of which are discussed in detail in our recent publication [20]. The metrics discussed for the films properties were: film formation capacity, film corrosion rate, film maintenance rate, film kinetic stability and film impedance. Overall, all phosphazene varieties improve cathode-electrolyte interface properties. All phosphazene varieties significantly reduce (by more than an order of magnitude) the impedance of SEIs on the anode, demonstrating an outstanding benefit for the phosphazene additives. For other SEIs properties, some are improved to different extents; some are not changed or slightly compromised.

3.4. Cycling performance

Full cell evaluation of each of the electrolyte chemistries of interest was performed using CR 2032-type coin cells. Electrolyte blends with baseline A were prepared with each of the FMs with concentrations of 5 and 20 wt%, while blends with baseline B were prepared with FM concentrations of 5, 10, 20, and 30 wt%. Three cells were constructed for each electrolyte blend. The cells were formed at a constant-current C/10 rate for three cycles with a 1 h rest between each charge and discharge cycle. The state of the cells was evaluated using a reference performance test (RPT) which consisted of constant-current discharges at C/10, C/3, and C/1 rates, with C/10 charges in between, followed by a 2-hr rest in between each complete cycle. The cells were cycled using C/10 charge rate followed by C/3 discharge rate for 40 cycles before another RPT cycle was run. The cells were cycled for a total of 200 cycles (excluding RPTs). The results of the first RPT performed after cell formation (*i.e.* beginning of life) are shown in Fig. 9. Each point in the figure is the average of 3 separate cells for each of the phosphazenes and its concentration in both of the baseline electrolytes. In both of the baselines, at slow discharge rates (C/10) addition of phosphazenes even up to 30% have little impact on cell capacity. While this is somewhat surprising given the higher viscosities and lower conductivities of the blends containing larger percentages of the phosphazenes, it does indicate that cell kinetic performance is not appreciably limited by electrolyte properties at this modest cycling rate. The exception to this is the performance of the 30% FM4 in baseline B which is significantly lower compared to other blends with the same phosphazene loading. This effect becomes apparent and more pronounced at higher discharge rates in both of the baselines. The decrease in capacity with higher phosphazene loading and faster discharge rates is most pronounced for FM4, followed by FM3, then FM2. FM2 performs as well as (and in some

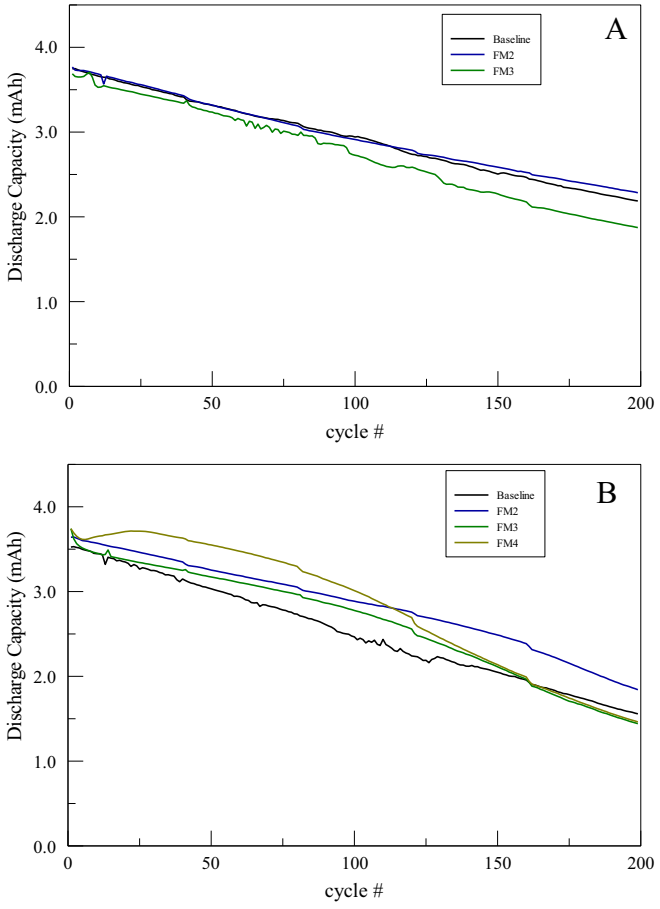

Fig. 10. Discharge cycle capacities as a function of cycle number for cells with 20 wt% of each of the phosphazenes in A) 1:1 EC:DEC with 1.0 M $LiPF_6$ and in B) 1:2 EC:EMC with 1.2 M $LiPF_6$ compared to the baseline electrolytes.

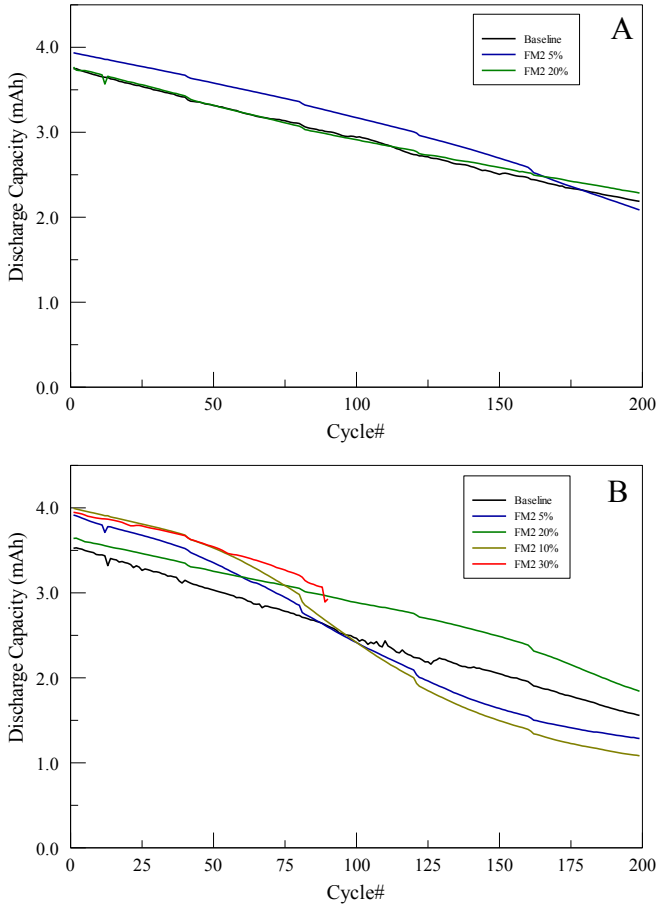

Fig. 11. Discharge cycle capacities as a function of cycle number for cells with FM2 at various concentrations in A) 1:1 EC:DEC with 1.0 M $LiPF_6$ and in B) 1:2 EC:EMC with 1.2 M $LiPF_6$ compared to the baseline electrolytes.

cases better than) the baseline until the highest concentrations and fastest discharge rate are reached (20% and 30% @ C/1).

In addition to determining the state of the cells after formation, the effects of cycle life were evaluated. Fig. 10 shows the discharge capacities for each of the electrolyte blends containing 20% phosphazene as a function of cycle number. In baseline A the initial capacities are all very high (~3.9 mAh). The capacities of the baseline and those with 20% phosphazene are very similar. The blend with FM3 shows a slightly higher capacity fade. In Fig. 10B, the capacities of 20% phosphazenes in baseline B are shown. All of the blends with the FMs show slightly higher capacities compared to the baseline. FM2 shows the best performance in the FM series and performs as well as or better than the baselines alone. The capacity fade for baseline B is a slightly more pronounced than for baseline A, perhaps due to the larger proportion of the more volatile EMC. Fig. 11 shows discharge capacities for blends containing various concentrations of FM2. In baseline A, the 5% FM2 showed the best performance, with discharge capacities superior to the baseline and the 20% FM2. In baseline B, all of the cells with FM2 showed higher initial capacities than the baseline, however there is not a systematic variation. After the first ~40 cycles the rates of capacity fade for the 5, 10, and 30% cells increases. In this baseline the best performance was from the 20% FM2.

It is noted that each of the conditions evaluated, including the baselines, exhibited capacity fade over the course of 200 cycles on the order of 25%. While significant, the decline for the baselines suggest that the fade is not related to electrolyte as the two chosen baselines have seen widespread using in energy storage systems. A more likely cause of the fade is improper balancing of the electrodes or gradual loss of capacity for the chosen electrodes. Both of these issues can be remedied in future work.

3.5. Electrochemical impedance spectroscopy (EIS)

In order to evaluate the properties of the solid electrolyte interphase (SEI), EIS spectra were obtained after cycling the cells for 160 cycles. Analysis of the EIS spectra (Fig. 12) shows key differences and similarities between the two electrolyte systems. The semicircles represent mechanistic processes that influence lithium transport between the free electrolyte region and the solid state domain, that is, the semicircles capture primarily interfacial attributes involving the charge transfer process, influence of SEI traits, and lithium desolvation. For both baselines there are changes in the interfacial impedance where for baseline A the impedance increases, but for B the impedance shows a decrease depending on the phosphazene additive. When comparing the same additive but employing different baselines it becomes apparent that irrespective of baseline the interfacial impedance and bulk impedance are uniform for each respective additive. Similar behavior is seen for FM3 and FM4. Such similarities within each group of additives strongly suggest that the interfacial character of the electrode surface films (SEI and cathode electrolyte interphase) is more strongly influenced by the respective phosphazene additives than by the bulk carbonate solvents in the electrolyte. Comparison of

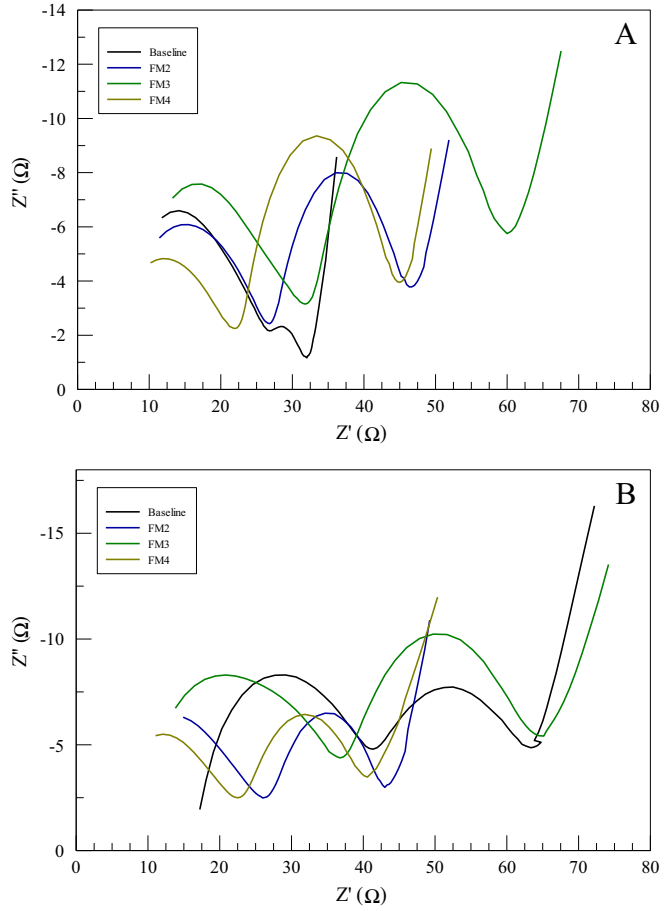

Fig. 12. Impedance spectra for cells containing 5 wt% phosphazenes in A) 1:1 EC:DEC with 1.0 M $LiPF_6$ and in B) 1:2 EC:EMC with 1.2 M $LiPF_6$ compared to the baseline electrolytes.

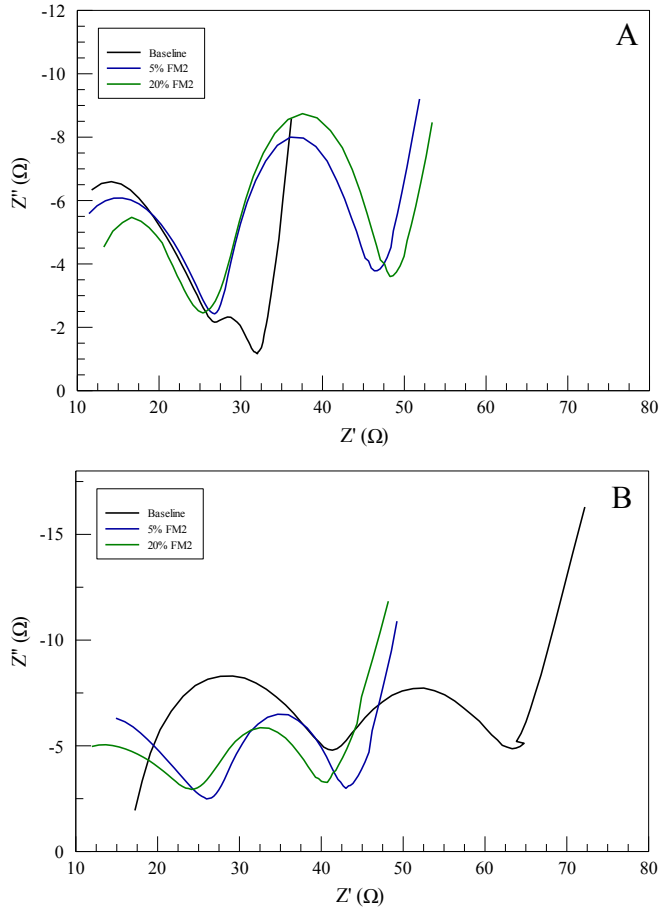

Fig. 13. Impedance spectra for cells containing 5 wt% and 20 wt% FM2 in A) 1:1 EC:DEC with 1.0 M $LiPF_6$ and in B) 1:2 EC:EMC with 1.2 M $LiPF_6$ compared to the baseline electrolytes.

loading level for FM2 (Fig. 13) indicate that loading level does not influence the bulk or charge transfer impedances regardless of baseline.

The lack of impedance shift within additive chemistries highlights the utility of phosphazenes as electrolyte additives. Of note is the ability to formulate electrolytes for specific purposes, such as lower viscosity, higher conductivity, decreased flammability and increased Li inventory without negatively impacting interphase behavior.

4. Conclusions

Phosphazenes are very promising for use as additives and co-solvents in lithium batteries employing alkyl carbonate electrolyte blends. While blends containing the phosphazenes had slightly lower conductivities and slightly higher viscosities, they also had increased flash points and lower vapor pressures. The most remarkable improvement in electrolyte properties that the phosphazenes showed was in the increased thermal and electrochemical stabilities. In thermal stability testing, not only were all of the phosphazenes in this series themselves stable but they also prevented the decomposition of the alkyl carbonates for both of the baseline blends tested. In addition to increased thermal stability, the phosphazenes also increased the electrochemical stability of the alkyl carbonate blend, widening the electrochemical window from 0.95 V to as high as 1.85 V. The increased thermal and electrochemical stabilities appear to be due primarily the phosphazene core as these effects were observed for all the phosphazenes and only varied slightly depending on the nature of the pendent groups.

In battery cell performance testing on newly formed cells, the phosphazenes (up to 30%) showed capacity performance as good as or even better than the baselines at slow cycling rates. At higher rates and at the higher concentrations of phosphazene, the discharge capacities were lower due the higher viscosities and the lower conductivities of these blends. Performance testing over the first 200 cycles of the cells showed the phosphazene samples had higher discharge capacities and showed less capacity fade than the baselines, with FM2 being the best performer. EIS spectra obtained after 160 cycles show the interfacial character of the electrode surface films is more strongly influenced by the respective phosphazene additives than by the bulk carbonate solvents in the electrolyte, thus allowing alkyl carbonate electrolytes to be tailored to optimize specific desired properties without affecting the interphase properties.

Acknowledgments

The authors gratefully acknowledge Peter Faguy and David Howell and the Office of Energy Efficiency and Renewable Energy, ABR Program within the United States Department of Energy. The authors also acknowledge support from the Idaho National Laboratory per contract DE-AC07-05ID14517.

References

[1] B. Scrosati, J. Garche, J. Power Sources 195 (2010) 2419–2430.
[2] W.A. Van Schalkwijk, B. Scrosati (Eds.), Advances in Lithium-ion Batteries, Kluwer Academic, New York, 2002.
[3] Y. Watanabe, S. Kinoshita, S. Wada, K. Hoshino, H. Morimoto, S. Tobishima, J. Power Sources 179 (2008) 770–779.
[4] A. Balducci, S. Jeong, G. Kim, S. Passerini, M. Winter, M. Schmuck, G. Appetecchi, R. Marcilla, D. Mecerreyes, V. Barsukov, V. Khomenko, I. Cantero, I. De Meatza, M. Holzapfel, N. Tran, J. Power Sources 196 (2011) 9719–9730.
[5] K. Yokoyama, S. Fujita, A. Hiwara, Y. Naruse, M. Toriida, A. Omaru, Non-aqueous Electrolytic Solutions and Non-aqueous Electrolyte Cells Comprising the Same, U.S. Patent 5,580,684, 1996.
[6] S.C. Narang, S.C. Ventura, B.J. Dougherty, M. Zhao, S. Smedley, G. Koolpe, Nonflammable/Self-extinguishing Electrolytes for Batteries, U.S. Patent 5,830,600, 1998.
[7] S.C. Narang, S.C. Ventura, P. Cox, Fabrication of electrodes and devices containing electrodes, U.S. Patent 6,168,885, 2001.
[8] N. Yoshimoto, Y. Niida, M. Egashira, M. Morita, J. Power Sources 163 (2006) 238–242.
[9] J. Arai, J. Electrochem. Soc. 150 (2003) A219–A228.
[10] J. Arai, J. Power Sources 119 (2003) 388–392.
[11] C. Chang, S. Hsu, Y. Jung, C. Yang, J. Power Sources 196 (2011) 9605–9611.
[12] Y.-G. Lee, J. Cho, Electrochim. Acta 52 (2007) 7404–7408.
[13] M. Xu, L. Zhou, L. Hao, L. Xing, W. Li, B. Lucht, J. Power Sources 196 (2011) 6794–6801.
[14] C.W. Lee, R. Venkatachalapathy, J. Prakash, Electrochem. Solid-State Lett. 3 (2000) 63–65.
[15] S. Sazhin, M. Harrup, K. Gering, J. Power Sources 196 (2011) 3433–3438.
[16] M. Benson, M. Harrup, K. Gering, Comput. Theor. Chem. 1005 (2013) 25–34.
[17] M. Harrup, K. Gering, H. Rollins, S. Sazhin, M. Benson, D. Jamison, C. Michelbacher, T. Luther, ECS Trans. 41 (2012) 13–25.
[18] M.K. Harrup, F.F. Stewart, J.R. Delmastro, T.A. Luther, Safe Battery Solvents, U. S. Patent #7,285,362, 2007).
[19] http://www.sigmaaldrich.com, 3/3/2014.
[20] S.V. Sazhin, K.L. Gering, M.K. Harrup, H.W. Rollins, J. Electrochem. Soc. 161 (2014) A393–A402.